Spectral-Transfer-Tensor Method for Characterizing Non-Markovian Noise

Yu-Qin Chen, Yi-Cong Zheng, Shengyu Zhang, and Chang-Yu Hsieh[*]

Tencent Quantum Laboratory, Tencent, Shenzhen, Guangdong 518057, China

With continuing improvements on the quality of fabricated quantum devices, it becomes increasingly crucial to analyze noisy quantum process in greater details such as characterizing the non-Markovianity in a quantitative manner. In this work, we propose an experimental protocol, termed spectral transfer tensor maps (STTMs), to accurately predict the Rivas-Huelga-Plenio non-Markovian measure of any Pauli channels without state preparation and measurement errors. In fact, for Pauli channels, STTM even allows the reconstruction of a highly precise noise power spectrum for qubits. At last, we also discuss how STTM can be useful to approximately characterize non-Markovianity of non-Pauli channels via Pauli twirling in an optimal basis.

I. INTRODUCTION

The past decade has witnessed a rapid development of quantum technologies, especially with the advent of the noisy intermediate-scale quantum (NISQ) era [1]. These achievements are firmly built upon our continually improving capability to fabricate, control, and benchmark quantum devices with unprecedented precision. Characterization protocols like quantum state and process tomography [2–6], randomized benchmarking (RB) [7–10], Hamiltonian learning [11–14], and quantum noise spectroscopy [15–18] have all proven to be instrumental in the diagnosis of faulty quantum devices and, eventually, help us build higher-quality devices. Recently, increasing attention has been turned toward more precise noise characterizations and control, such as detecting and suppressing non-Markovian noises, which bears implications to other characterization protocols such as RB that assumes Markovian noises. Despite these recent efforts, there is still no state preparation and measurement (SPAM) error-free method to efficiently quantify strength of non-Markovian noises in a quantum device. In this work, we propose such a method by combining a recently proposed transfer tensor method [19,20] and the spectral quantum process tomography [21].

Quantum devices are often operated in a noisy environment. If the noise is Markovian, it is straightforward to predict the adverse effects and manipulate quantum states as desired. When non-Markovian memory plays a critical role, the associated quantum dynamics becomes significantly harder to analyze and control as the dynamical evolution is intimately affected by the past trajectory. This challenge could even create nontrivial roadblocks for

building a fault-tolerant quantum computer. Hence, as we attempt to increase the scale of a quantum device, such as the circuit depth and qubit counts of a quantum circuit, it is desirable to quantify and suppress non-Markovian noises.

Currently, there are many competing proposals for non-Markovianity measures due to different perspectives and motivations. This is an active research area, and no unanimous consensus on the most useful measure (for developing quantum technology) has been reached. Among them, the Rivas-Huelga-Plenio (RHP) measure is inspired by the violation of completely positive (CP) divisibility for non-Markovian dynamical maps. While RHP is a mathematically rigorous approach, it is not straightforward to deduce in experiments. The challenge is further aggravated by the need to remove SPAM errors in order to achieve high-precision measurements for a quantum hardware. As elucidated later, we propose a SPAM error-free experimental method and rigorously deduce RHP measure from a set of spectral quantum process tomographies (SQPTs) [21] for any Pauli channels and a bounded approximate on the RHP measure for other non-Pauli channels.

Quantum process tomography (QPT) [4–6] is among the most widely used tool for experimentally characterizing quantum dynamics and has been used in the context of quantum technology, such as determining quantum gate fidelities [22–24] and investigating environment-induced errors [25,26]. However, earlier theoretical and experimental efforts [26,27] were largely confined to device characterization without taking non-Markovianity of noise into account. A newly proposed method, transfer tensor map (TTM) [19,28], offers a way to bridge experimentally deduced QPT data with the theory of time-nonlocal quantum master equation (TNQME) [29], which is valid for general open quantum dynamics including non-Markovian

ones. Built upon the theory-experiment connection under the TTM framework, Ref. [20] further proposes a suite of experimental protocols to more easily (1) witness the non-Markovianity of a quantum process, (2) reconstruct the noise power spectrum, and (3) estimate spatial and temporal correlations of nonlocal noise in a quantum device.

In this work, we replace the standard QPT experiments considered in Ref. [20] with the newly proposed SQPT [21], which gives SPAM error-free estimates of eigenvalues of quantum channels. The original SQPT is most appropriate for characterizing Markovian quantum channels. In the original proposal [21], non-Markovian noises can only be detected but not quantified. Combining SQPT with TTM, we derive a spectral form of TTM, dubbed STTM, that allows us to quantify degrees of non-Markovianity for any Pauli channels. With limited efforts, one can further extract the noise power spectrum for these channels. For more general quantum processes beyond Pauli channels, we apply Pauli twirling in an optimal basis (as defined in a later section) to estimate the degree of non-Markovianity. Without loss of generality, we describe the proposed STTM in the context of characterizing qubits in a circuit model. We note that the effort to simultaneously reduce the experimental costs of quantum process tomography and make it compatible with SPAM error free is a highly nontrivial challenge. The present method (building upon SQPT) is only valid for a high-quality quantum hardware satisfying certain conditions detailed in Appendix B. In short, it works best if the environment can be modeled as a source of classical noise or the environment has a fast reorganization and only weakly coupled to the system. To extend the present method to work with more general environments, we may further incorporate the theoretical framework of Ref. [30]

The remainder of this work is organized as follows. Section II summarizes the derivation of spectral transfer tensor maps. Section III discusses the proposed STTM noise spectroscopy. Section IV discusses an extension of STTM to non-Pauli channel. Section V describes the usage of STTM noise spectroscopy with examples based on theoretical models. Section VI concludes.

II. SPECTRAL TRANSFER TENSOR METHOD FOR PAULI CHANNELS

The STTM is an elegant combination of TTM and SQPT for characterizing Pauli channels. We first recap these two methods before we present our contribution, STTM, which draws inspirations from both methods to efficiently investigate non-Markovian dynamics without influences of SPAM errors. This high-precision analysis should provide essential information to further improve the quality of existing quantum devices.

A. Transfer tensor maps

We first review the theory of TTM as originally formulated in Ref. [19]. The most general dynamical evolution of an open quantum system is given by

$$\rho_t = \left\langle \exp_+\left(-i\int_0^t dsH(s)\right)\rho_0\rho_B\exp_-\left(i\int_0^t dsH(s)\right)\right\rangle$$
$$= \Lambda_t\rho_0, \tag{1}$$

where ρ_B is the initial state of the environment, $H(t)$ is the total Hamiltonian of a time-dependent system comprising a system and its environment. The $\pm$ subscript denotes the (anti)chronological time ordering of the time-evolution operator. The bracket $\langle\cdots\rangle$ denotes an average over the environmental degrees of freedom. Λ_t is the dynamical map relating the initial density matrix to the time-evolved reduced density matrix. The dynamical maps Λ for a d-level quantum system are derived from an ensemble of QPTs obtained under d^2 different initial conditions. In an experiment, the QPTs are supposedly performed at equidistant time intervals, i.e., $t_k = k\delta t$, thus $\Lambda_k \equiv \Lambda_{t_k}$.

If we assume a separable system-bath initial condition and a time-independent Hamiltonian then an open system's dynamics can be succinctly cast in the form,

$$\rho_{t_n} = \sum_{m=1}^n T_m\rho_{t_{n-m}}, \tag{2}$$

where the system's state at time t_n is determined by the history of its past evolution extending all the way back to t_0. In Eq. (2), TTMs T_m are introduced to correlate two density matrices ρ_{t_n} and $\rho_{t_{n-m}}$. More specifically, TTMs are defined via

$$T_n \equiv \Lambda_n - \sum_{m=1}^{n-1} T_{n-m}\Lambda_m, \tag{3}$$

with $T_1 = \Lambda_1$. Time translational invariance of the dynamical process is implicitly assumed, as these maps are related by the time difference $m\delta t$.

For most practical cases, one can approximate exact quantum dynamics by truncating the TTM series to a finite number of terms, i.e., $\{T_1, \ldots, T_M\}$ in Eq. (2). This observation is the key that the TTM formalism could be useful in an actual experiment, as one only needs to perform M QPTs to deduce the dynamical maps $\{\Lambda_1, \ldots, \Lambda_M\}$ and associated TTMs. Beyond t_M, all quantum dynamical information can be recursively predicted with the help of TTMs via Eqs. (2)–(3).

B. Spectral quantum process tomography

SQPT [21] is another developed tomographic technique that provides only partial information (eigenvalues of a quantum channel) on the dynamical processes under investigation. SPAM-resistant protocols must make a certain trade-off between characterization details and efficiency. For instance, a scalable method like RB may only output a scalar number to benchmark the gate quality. On the other hand, methods like robust tomography and gate-set tomography characterize all aspects of a quantum gate at the expense of scalability. Aforementioned examples are extreme cases, and SQPT situates in the middle of the spectrum. It gives SPAM error-free estimates on the spectral properties of a quantum gate without consuming as much resources as the standard QPTs, which are SPAM error prone. Furthermore, it does not require complex experimental protocols for implementations. We briefly summarize the idea of SQPT below.

Any completely positive and trace-preserving (CPTP) map Λ acting on density operators in a d-dimensional Hilbert space for an n-qubit system can be represented with a corresponding Pauli transfer matrix,

$$S_{\mu\nu} = \text{Tr}\left[P_\mu \Lambda \left(P_\nu \right) \right], \quad \mu, \nu = 0, \ldots, N, \quad (4)$$

where $P_0 = I^{\otimes n}$, $P_1 = I^{\otimes n-1} \otimes X$, $P_2 = I^{\otimes n-1} \otimes Y, \ldots$, $P_N = Z^{\otimes n}$ are Pauli matrices with $N = d^2 - 1$ and $d = 2^n$. If we are restricted to dealing with unital channels, i.e., $\Lambda(I) = I$, then the Pauli transfer matrix assumes a block-diagonal form,

$$S = \begin{pmatrix} 1 & 0 \\ 0 & R \end{pmatrix}. \quad (5)$$

The SQPT protocol relies on an observation that eigenvalues of R matrix in Eq. (5) may be deduced from a set of experimentally generated signal functions $\{g(1), g(2), \ldots, g(K)\}$, where $K \geq 2N - 2$ in order to determine the eigenvalues accurately. These signal functions are defined as

$$g(k) = \frac{1}{2^n} \sum_{\mu=1}^{N} \text{Tr}\left[P_\mu \mathcal{N}_m \circ \Lambda^k \circ \mathcal{N}_p \left(P_\mu \right) \right],$$

$$= \frac{1}{2^n} \text{Tr}\left[R_{\text{meas}} R^k R_{\text{prep}} \right],$$

$$= \frac{1}{2^n} \text{Tr}\left[A_{\text{SPAM}} D^k \right] = \frac{1}{2^n} \sum_{j=1}^{N} A_j \lambda_j^k, \quad (6)$$

where $\mathcal{N}_p$, Λ^k, and $\mathcal{N}_m$ are quantum channels corresponding to the state-preparation error, k-fold applications of a unitary operation, which is generalized to a CPTP map when accounting for noise decoherence, and measurement

errors, respectively. The first line of Eq. (6) gives a clear experimental procedure to construct the signal functions: preparing an eigenstate of P_μ operator, apply a target unitary k times, and perform projective measurement in the P_μ-diagonal basis. Finally, this procedure is repeated for different eigenstate of P_μ and for different μ index as indicated in the summation appearing on the right-hand side of the first line of Eq. (6).

As we focus on unital channels, the second line of Eq. (6) immediately follows. R_{meas} and R_{prep} are the R submatrix of Pauli transfer matrix for $\mathcal{N}_m$ and $\mathcal{N}_p$, respectively. The R submatrix of a target unitary $R = VDV^{-1}$ can be diagonalized. Under the trace operation, we may shuffle V and V^{-1} to obtain $A_{\text{SPAM}} = V^{-1} R_{\text{meas}} R_{\text{prep}} V$, which captures all SPAM errors, in the third line. As D^k is a diagonal matrix with entries λ_j^k we end up with a simple interpretation of $g(k)$, i.e., it is proportional to $\sum_{j=1}^{N} A_j \lambda_j^k$. By using the matrix-pencil method to postprocess the time series of $\{g(1), \ldots, g(K)\}$, one may reliably extract λ_j.

C. Pauli channels

The family of Pauli channels represents a wide class of noise processes including several prominent decoherence models for quantum computations, such as the depolarizing, dephasing, bitflip, and amplitude damping channels. A Pauli channel can be described by a Pauli map [31,32]. For one-qubit cases, a general Pauli channel assumes the following form:

$$\Lambda[\rho] = \sum_{\alpha = \{0, x, y, z\}} f_\alpha P_\alpha \rho P_\alpha, \quad (7)$$

where $P_0 = \mathbb{I}_2$ and $\{P_\alpha | \alpha = x, y, z\}$ are the Pauli operators. The coefficients f_α collectively satisfy a simple relation $\sum_{\alpha = \{0, x, y, z\}} f_\alpha = 1$. These maps have eigenvalues λ_α as defined by

$$\Lambda\left[P_\alpha \right] = \lambda_\alpha P_\alpha, \quad (8)$$

with $\lambda_0 = 1$. There is a simple relation between f_α and λ_α, namely,

$$\lambda_\alpha = \sum_{\beta = \{0, x, y, z\}} (-1)^{s([P_\beta, P_\alpha])} f_\alpha, \quad \alpha = x, y, z, \quad (9)$$

where $s([P_\beta, P_\alpha]) = 0$ if $[P_\beta, P_\alpha] = 0$ and $s([P_\beta, P_\alpha]) = 1$ otherwise. A Pauli map is completely positive if and only if its eigenvalues satisfy the Fujiwara-Algoet conditions [33]

$$|1 \pm \lambda_z| \geqslant |\lambda_x \pm \lambda_y|. \quad (10)$$

D. Spectral quantum process tomography for non-Markovian dynamics

The original SQPT reviewed above works naturally for a Markovian channel, but not directly applicable to non-Markovian ones. This is because a non-Markovian channel violates divisibility,

$$\Lambda_{m+n} \neq \Lambda_m \Lambda_n, \tag{11}$$

where $\Lambda_m \equiv \Lambda_{t_m}$. Recall that, under the standard SQPT framework, $g(k)$ signals are treated as a time series $\{t_0, t_1, \ldots, t_k, \ldots\}$ spaced with a uniform interval δt. If the quantum channel under interrogation is a Markovian process, then $\Lambda_{t_k} = \Lambda_{\delta t}^k$, which is implicitly assumed in Eq. (6). Non-Markovian channels no longer fit into the original framework that extracts spectral properties of a dynamical process from the signal function $g(k)$ by using the matrix pencil method. In this subsection, we propose a method to generalize the original framework for non-Markovian Pauli channels.

To address this deficiency, we redefine the signal functions. As the quantum channel is not divisible, we simply take every Λ_n as an independent channel and introduce a subscript t_n to the signal function, i.e.,

$$g_{t_n}(k) = \frac{1}{2^n} \sum_{\mu=1}^{N} \text{Tr} \left[P_\mu \mathcal{N}_m \circ \Lambda_n^{(k)} \circ \mathcal{N}_p \left(P_\mu \right) \right]. \tag{12}$$

The modified signal function carries two "time" labels: operational time duration t_n to denote the quantum channel Λ_n under investigation, and logical time duration k to imply the artificially constructed dynamical processes Λ_n^k, which are required for the matrix-pencil method to extract the spectrum of Λ_n via K time points of the signals $\{g_{t_n}(1), \ldots, g_{t_n}(K)\}$.

If one is interested in characterizing a non-Markovian process up to time $t_M = M\delta t$, then one needs to construct M independent sets of signal functions $\{g_{t_n}(1), \ldots g_{t_n}(K) \mid n = 1, \ldots, M\}$. For each set of signal functions, one applies the standard STTM to deduce the time-evolved spectrum of Λ_n from K logical time points,

$$\left\{ \{\lambda_1^{(1)}, \lambda_2^{(1)}, \ldots\}, \{\lambda_1^{(2)}, \lambda_2^{(2)}, \ldots\}, \ldots, \{\lambda_1^{(M)}, \lambda_2^{(M)}, \ldots\} \right\}, \tag{13}$$

where $\lambda_m^{(n)}$ denotes the mth eigenvalues for Λ_n. A number of useful properties can be inferred from these spectra, such as the degrees of non-Markovianity and noise power spectrum as elucidated later in the text. See Fig. 1 for a brief summary.

While it is obvious that $g_{t_n}(k)$ in Eq. (12) is a generalization of Eq. (6) for non-Markovian processes, it is not easy to experimentally construct $g_{t_n}(k)$. Next, we propose an experimental protocol to extract spectra of non-Markovian

FIG. 1. (a) A sequence of signal functions to extract dynamical spectral for Markovian noise. (b) Group of the sequence of signal functions needed to extract dynamical spectral for non-Markovian noise.

Λ_n spanning a duration $T = n\delta t$. The proposed protocols requires us to perform two sets of experiments, delineated in Figs. 2(a) and (b), respectively. In this figure, symbol Λ_n denotes the targeted quantum channel, **P** denotes the state-preparation circuit to create an eigenstate of an n-qubit Pauli matrix P_μ, and **M** corresponds to a projective measurement in the eigenbasis of P_μ.

Figure 2(a) implies a set of simple circuits in which Λ_n and **M** are interleaved for $k = 1, 2, 3, \ldots$ times. If one repeats the experiments in (a) to cover all possible initial state preparations and measurements in the Pauli basis,
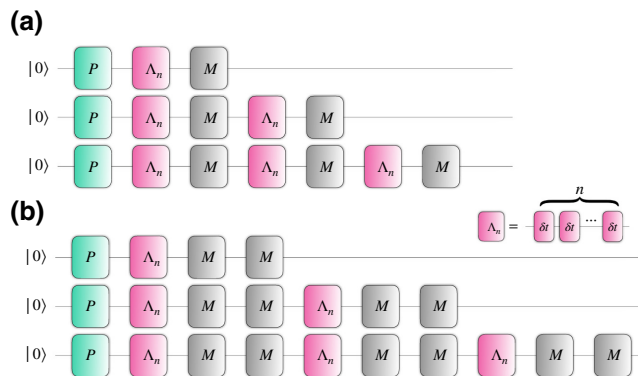

FIG. 2. Protocol to capture signal functions for non-Markovian noise. Λ_n is the concerned quantum channel corresponding to dynamical map of various evolution time t_n. "**M**" is the projection measurement in the same direction of initial Pauli matrix. (a) Alternately apply concerned quantum channel and projection measurement. (b) Alternately apply concerned quantum channel and double projection measurements.

then one may construct a signal function,

$$
\begin{aligned}
g'_{t_n}(k) &= \frac{1}{2^n} \sum_{\mu=1}^{N} \mathrm{Tr}\left[P_\mu \mathcal{N}_m \circ \Lambda_n \circ \left(M_\mu \circ \mathcal{N}_m \circ \Lambda_n \right)^{k-1} \right. \\
&\qquad \left. \circ \mathcal{N}_p \left(P_\mu \right) \right] \\
&= \frac{1}{2^n} \sum_{\mu=1}^{N} \mathrm{Tr}\left[P_\mu \left(\mathcal{N}_m \circ \Lambda_n \right)^k \circ \mathcal{N}_p \left(P_\mu \right) \right] \\
&= \mathrm{Tr}\left[\left(R_{\mathrm{meas}} R_{\mathrm{dyn}} \right)^k R_{\mathrm{prep}} \right] \\
&= \mathrm{Tr}\left[A_P D^k \right] = \sum_{j=1}^{N} A_j \left(m_j \lambda_j^{(n)} \right)^k,
\end{aligned}
\tag{14}
$$

where R_{meas}, R_{dyn}, and R_{prep} are the submatrix R of the Pauli transfer matrix for $\mathcal{N}_{\mathrm{meas}}$, Λ_n, and $\mathcal{N}_{\mathrm{prep}}$, respectively. $R_{\mathrm{meas}} R_{\mathrm{dyn}} = V D V^{-1}$ can be diagonalized with eigenvalues $\tilde{\lambda}_j^{(n)} = m_{s(j)} \lambda_j^{(n)}$, where m_s and $\lambda_j^{(n)}$ are eigenvalues of R_{meas} and R_{dyn}, respectively. This special relation (spectra of a matrix product is derived from multiplications of the spectrum of two matrices) holds for Pauli channels. $A_P = V^{-1} R_{\mathrm{prep}} V$ encapsulates all the state-preparation errors. As every application of dynamical map Λ_n is followed with a projective measurement, the fundamental components that scale with k are actually $(m_{s(j)} \lambda_j^{(n)})^k$. Hence, applying the matrix-pencil method to the time series constituted by K signal functions, $g'_{t_n}(k)$, would give us an estimate of $m_{s(j)} \lambda_j^{(n)}$ instead. To isolate $\lambda_j^{(n)}$, we need additional equations. Hence, we propose to perform a second set of experiments delineated in Fig. 2(b). In this case, the experiment protocol is almost identical to the previous experiment except that every application of a dynamical map Λ_n is followed by two consecutive projective measurements. Now, one may construct a set of signal functions,

$$
\begin{aligned}
g''_{t_n}(k) &= \frac{1}{2^n} \sum_{\mu=1}^{N} \mathrm{Tr}\left[P_\mu \mathcal{N}_m \circ M'_\mu \circ \Lambda_n \circ \left(M'_\mu \circ M'_\mu \circ \Lambda_n \right)^{k-1} \right. \\
&\qquad \left. \circ \mathcal{N}_p \left(P_\mu \right) \right] \\
&= \frac{1}{2^n} \sum_{\mu=1}^{N} \mathrm{Tr}\left[P_\mu \left(\mathcal{N}_m \circ \mathcal{N}_m \circ \Lambda_n \right)^k \circ \mathcal{N}_p \left(P_\mu \right) \right] \\
&= \mathrm{Tr}\left[\left(R_{\mathrm{meas}} R_{\mathrm{meas}} R_{\mathrm{dyn}} \right)^k R_{\mathrm{prep}} \right] \\
&= \mathrm{Tr}\left[A_P D^k \right] = \sum_{j=1}^{N} A_j \left(m_j^2 \lambda_j^{(n)} \right)^k.
\end{aligned}
\tag{15}
$$

where $M'_\mu = M_\mu \circ \mathcal{N}_m$. $R_{\mathrm{meas}} R_{\mathrm{meas}} R = V D V^{-1}$ is diagonal, $A_P = V^{-1} R_{\mathrm{prep}} V$ captures preparation error. It is clear

that the matrix-pencil method may give us an estimate of $(m_{s(j)}^2 \lambda_j^{(n)})$, which are eigenvalues of $R_{\mathrm{meas}}^2 R_{\mathrm{dyn}}$. Now, by combining the experimental results of these two sets of experiments, we can easily obtain

$$
\lambda_j^{(n)} = \frac{\left(m_j \lambda_j^{(n)} \right)^2}{m_j^2 \lambda_j^{(n)}}.
\tag{16}
$$

If we perform these two sets of experiments, Figs. 2(a) and (b), to deduce the time-evolved spectra, $\lambda_j^{(n)}$ for $n = 1, \ldots, M$ without SPAM errors. We note that for the readout errors of moderate strength, eigenvalues for g' and g'' will maintain the same order and make Eq. (16) feasible.

E. Spectral transfer tensor method

We now introduce STTM for Pauli channels. We discuss how the method can be useful for more general dynamical processes in Sec. IV B.

Since Pauli channels necessarily have a diagonal Pauli transfer matrix in a fixed basis for all time, it can be proved inductively that T_n derived from Eq. (3) must be diagonal in the same basis. The non-Markovian SQPT described in the previous subsection can be invoked to give diagonal elements for Λ_m. Via Eq. (2), one may recursively derive the following relations:

$$
\lambda_n^\alpha = \sum_{m=0}^{n-1} \tau_{n-m}^\alpha \lambda_m^\alpha,
\tag{17a}
$$

$$
\tau_n^\alpha = \lambda_n^\alpha - \sum_{m=1}^{n-1} \tau_{n-m}^\alpha \lambda_m^\alpha,
\tag{17b}
$$

where τ_n^α denotes an eigenvalue of T_n. In this work, we refer to the set $\{\tau_n^\alpha \mid \alpha \in \{x, y, z\}$ and $n = 1, \ldots, M\}$ as the STTM. As discussed before, it is often appropriate to assume the memory kernel of a non-Markovian process has finite width and truncate the summation in Eq. (17a) by keeping the first M terms and discarding the rest.

F. Resource consumption

Finally, we analyze the efforts required to implement STTM based on the protocols introduced in Fig. 2. According to Eqs. (14)–(15), each of these two modified signal functions requires the same amount of experimental efforts as the original SQPT. Since STTM requires a characterization of M dynamical maps to cover the memory kernel, there is a total of $d \times (d^2 - 1) \times (K + 1) \times M$ distinct experiments (i.e., quantum circuits). Each distinct experimental setup should be further repeated N_{samples} times in order to reach an acceptable variance $\propto \mathcal{O}(1/N_{\mathrm{samples}})$ for the measurement statistics. While the present approach is not scalable, it is still a more economical approach

(when $d \gg K$) to obtain the SPAM-free estimate of a memory kernel for a non-Markovian Pauli channel. If we compare STTM to a more direct application of SPAM-free process tomographic technique, such as the gate-set tomography, to derive TTM for the same quantum system. Gate-set tomography would require $d^2 \times (d^2 - 1) \times M$ distinct experiments.

III. NOISE SPECTROSCOPY BASED ON STTM

In this section we further discuss how STTM can be used to (1) quantify non-Markovianity and (2) reconstruct power spectrum for Pauli channels. Before delving into these tasks, we first relate the spectral properties of a Pauli channel to the corresponding time-local and nonlocal master equations.

A. Master equations for Pauli channels

Dynamics for every open quantum system can be described by the Nakajima-Zwanzig equation,

$$\dot{\rho}_t = -i\mathcal{L}_s\rho(t) + \int_0^t \mathcal{K}_{t-t'}\rho_{t'}dt', \quad (18)$$

where $\mathcal{L}_s$ is the Liouvillian of the system alone, $\mathcal{K}_t$ is the non-Markovian memory kernel that relates a system's past dynamical history to its present evolution under the influence of an external environment such as noise. In addition to Eq. (18), the dynamical evolution can be alternatively represented in a time-local form as follows:

$$\dot{\rho}_t = \left(\int_0^t \mathcal{K}_{t-t}\Lambda_{t'}\Lambda_t^{-1}dt' \right) \rho(t) \equiv \mathcal{L}_t\rho(t). \quad (19)$$

For Pauli channels Λ_t, that is diagonal in the Pauli basis, one immediately infers that both $\mathcal{L}_t$ and $\mathcal{K}_t$ are also diagonal in the Pauli basis for all time t. In fact, one can explicitly show that

$$\mathcal{K}_t = \sum_{\alpha=x,y,z} k_\alpha(t)[\mathbb{U}_\alpha - \mathbb{I}],$$

$$\mathcal{L}_t = \frac{1}{2} \sum_{\alpha=x,y,z} \gamma_\alpha(t) [\mathbb{U}_\alpha - \mathbb{I}], \quad (20)$$

where $\mathbb{U}_\alpha[\rho] = P_\alpha\rho P_\alpha^\dagger$ and $\mathbb{I}[\rho] = \rho$. Hence, the dynamical evolution of a Pauli channel is also fully encapsulated in the parameters $k_\alpha(t)$ and $\gamma_\alpha(t)$. To quantify non-Markovianity and reconstruct the noise power spectrum of a non-Markovian dynamics, it is beneficial to have $k_\alpha(t)$ and $\gamma_\alpha(t)$ readily extracted from experiments.

Casting the Nakajima-Zwanzig equation $\dot{\rho}(t_n) = \sum_{m=0}^{n-1} \mathcal{K}_{n-m}\rho(t_m)\delta t$ in a discretized form, one may relate the

memory kernel to the TTMs in Eq. (2) if these maps are sampled at sufficiently small time step δt,

$$T_n = \mathcal{K}_n\delta t^2 + \delta_{n,1}. \quad (21)$$

Noting the TTM and the memory kernel in Eq. (21) should assume a diagonal form for Pauli channels, we immediately obtain

$$k_n^\alpha \delta t^2 = \tau_n^\alpha - \delta_{n,1}. \quad (22)$$

This relation above indicates that one may readily reconstruct the memory kernel from STTM with minimal efforts.

Next, the generator for a Pauli channel must satisfy

$$\mathcal{L}_t[P_\alpha] = \mu_\alpha(t)P_\alpha, \quad (23)$$

with $\mu_\alpha(t) = \gamma_\alpha(t) - \sum_{\beta=\{x,y,z\}} \gamma_\beta(t)$. From Eq. (19), we may deduce

$$\dot{\Lambda}_t[P_\alpha] = \mathcal{L}_t\Lambda_t[P_\alpha], \quad (24)$$

and draw the conclusion that $\lambda_\alpha(t) = \mathrm{Exp}\left[\int_0^t \mu_\alpha(\tau)d\tau \right]$. Thus, we acquire a relationship between $\gamma_\alpha(t)$ and λ_α as follows:

$$\Gamma_t = \int_0^t \gamma_\alpha(\tau)d\tau = \frac{1}{2} \ln \frac{\lambda_\alpha(t)}{\lambda_\beta(t)\lambda_\eta(t)}, \quad \alpha \neq \beta \neq \eta. \quad (25)$$

With help of STTM via Eq. (17a), we may estimate Γ_t for all time t.

B. RHP measure for Non-Markovianity

A mathematically rigorous measure for non-Markovianity of a dynamical process was proposed by Rivas, Huelga, and Plenio [34]. This measure is motivated by the fact that a local Markovian dynamics always leads to a monotonic decrease of the entanglement between a system and an ancilla of the same dimension while non-Markovianity (violate the CP divisibility) induces a temporary reversal of this diminishing trend. Hence, the rate of change of the bipartite entanglement gives a concrete way to quantify non-Markovianity. More precisely, the RHP measure proposes that one should follow the rate of entanglement change for a bipartite system initialized in a maximally entangled state $\rho = |\Phi\rangle\langle\Phi|$ and evolves under the quantum channel $\Lambda_t \otimes I[\rho]$,

$$\mathcal{I} = \int_0^\infty \mathbf{g}(t)dt, \quad (26)$$

with

$$\mathbf{g}(t) = \lim_{\epsilon \to 0^+} \frac{\| [I + (\mathcal{L}_t \otimes I)\epsilon] |\Phi\rangle\langle\Phi| \|_1 - 1}{\epsilon}, \quad (27)$$

where $|| \cdot ||_1$ denotes the trace norm, $\mathcal{L}_t$ is the generator of Λ_t as defined in Eq. (19). For Pauli channels, a

straightforward calculation leads to

$$\mathbf{g}_\alpha(t) = \begin{cases} 0 & \text{for} \quad \gamma_\alpha(t) \geqslant 0 \\ -\gamma_\alpha(t) & \text{for} \quad \gamma_\alpha(t) < 0 \end{cases} \qquad (28)$$

and finally

$$\mathcal{I} = \sum_{\alpha=\{x,y,z\}} \mathcal{I}_\alpha = \sum_{\alpha=\{x,y,z\}} \int_{\gamma_\alpha(t)<0} -\gamma_\alpha(t)dt. \qquad (29)$$

Thus, an accumulation of negative decoherence rates $\gamma_\alpha(t)$ over the duration $t \in [0,\infty]$ accounts for non-Markovianity. According to Eq. (25), decoherence rates are related to the spectra of dynamical maps that can be deduced from STTM for an arbitrary long time.

C. Noise power spectrum

Next we describe how the STTM allows one to reconstruct the noise power spectrum for an open quantum system. Let us consider a set of qubits governed by the following Hamiltonian:

$$H(t) = H_s + H_{sb}(t)$$
$$= H_s + \sum_{i,\alpha} g_i B_i^\alpha(t)\sigma_i^\alpha, \qquad (30)$$

where H_s is a time-independent system Hamiltonian for the qubits, and H_{sb} denotes the system-noise interaction. σ_i^α is a Pauli operator with the index i labeling the qubits and the index α one of the $\{x,y,z\}$ Cartesian components. $B_i^\alpha(t) = e^{-iH_b t}B_i^\alpha(0)e^{iH_b t}$ is a bath operator in the interaction picture with respect to H_b, the environment Hamiltonian. If assuming Gaussian noises, then the environment-induced perturbations can be fully captured in the first two statistical moments $\langle B_i^\alpha(t)\rangle$ and $\langle B_i^\alpha(t)B_j^\beta(t')\rangle$ with $\langle \cdot \rangle$ implying an average with ρ_b, such as the thermal state for the bath.

For a piece of high-quality quantum hardware, it is often sufficient to consider the weak-coupling regime for system-noise coupling. The exact memory kernel [29] for an arbitrary quantum bath can be written as follows:

$$\mathcal{K}(t,t') = \mathcal{P}\mathcal{L}(t)\exp_+\left[\int_{t'}^t ds\,\mathcal{Q}\mathcal{L}(s)\right]\mathcal{Q}\mathcal{L}(t')\mathcal{P}, \qquad (31)$$

where projection operators $\mathcal{P}$ and $\mathcal{Q} = 1 - \mathcal{P}$ are defined by $\mathcal{P}\Omega(t) = \mathrm{Tr}_b[\Omega(t)] \otimes \rho_b$, i.e., $\mathcal{P}$ projects a system-bath entangled quantum state $\Omega(t)$ to a factorized form consisting of a system part $\rho(t) = \mathrm{Tr}_b\Omega(t)$, and a bath part ρ_b, which is a stationary state with respect to the bath Hamiltonian H_b. We note that the kernel is a stationary process $\mathcal{K}(t,t') = \mathcal{K}(t-t')$ when the noise satisfies the stationary Gaussian conditions.

The memory kernel for a Gaussian noise can be expressed as $\mathcal{K}(t) = \sum_{n=1}^\infty \mathcal{K}_{2n}(t)$, where $\mathcal{K}_{2n}(t)$ corresponds to the order $2n$ expansion of the Hamiltonian with

respect to H_{sb}. Keeping only the leading (i.e., second-order) term gives

$$\mathcal{K}(t)(\cdot) \approx \mathcal{K}_2(t)$$
$$= \sum_{\alpha\alpha'}[\sigma^\alpha, C_{\alpha\alpha'}(t)\sigma^{\alpha'}(t)(\cdot) - C_{\alpha\alpha'}^*(t)(\cdot)\sigma^{\alpha'}(t)], \qquad (32)$$

where $\sigma^\alpha(t) = \exp(-iH_s t)\sigma^\alpha \exp(iH_s t)$ and the bath correlation functions are given by

$$C_{\alpha\alpha'}(t) = g^2\left\langle \hat{B}^\alpha(t)\hat{B}^{\alpha'}(0)\right\rangle. \qquad (33)$$

We suppress the index i on Pauli matrices and noise operators $\hat{B}^\alpha(t)$ in Eqs. (32)–(33), as we should illustrate the idea with a one-qubit case from here onward.

For the Pauli channel defined in Eq. (7), the weak-coupling (second-order approximated) memory kernel reads

$$\mathcal{K}(t)\rho(t) = \sum_{\alpha=x,y,x} \left[C_{\alpha\alpha}(t) + C_{\alpha\alpha}^*(t)\right](\sigma_\alpha \rho(t)\sigma_\alpha - \rho(t)). \qquad (34)$$

On the other hand, the memory kernel of a Pauli channel is known to possess a simple expression,

$$\mathcal{K}_t = \sum_{\alpha=x,y,z} \frac{1}{2}k_\alpha(t)\left[\mathbb{U}_\alpha - \mathbb{I}\right]. \qquad (35)$$

Relating Eqs. (34) and (35), we identify a way to reconstruct $C_{\alpha\alpha}(t)$ from STTM data [via first calculating $k_\alpha(t)$ as discussed in a previous section],

$$k_\alpha(t_n) = 2\left[C_{\alpha\alpha}(t_n) + C_{\alpha\alpha}^*(t_n)\right]$$
$$- \sum_{\beta=x,y,x} 2\left[C_{\beta\beta}(t_n) + C_{\beta\beta}^*(t_n)\right]. \qquad (36)$$

Once the noise correlation function is determined, the corresponding spectral density can be determined by invoking the fluctuation-dissipation theorem [35], which gives

$$J_{\alpha\alpha}(\omega) = \frac{1}{2}\int_{-\infty}^\infty dt\,e^{i\omega t}\left[C_{\alpha\alpha}(t) - C_{\alpha\alpha}^*(t)\right]. \qquad (37)$$

IV. BEYOND PAULI CHANNEL

In the previous sections, we introduce STTM for non-Markovian Pauli channels. For more general dynamical processes, we suggest to apply the Pauli twirling approximation (PTA) in order to extract useful information. This is a much more challenging task. While one may derive a rigorous witness of non-Markovianity under the PTA, it is more realistic to obtain an estimated quantification of the degree of non-Markovianity for non-Pauli channels.

A. Pauli twirling approximation

According to Ref. [36], a quantum channel Λ can be approximated by a Pauli channel $\tilde{\Lambda}$ through PTA,

$$
\begin{aligned}
\tilde{\Lambda}(\rho) &= \frac{1}{K} \sum_{v=0}^{K-1} P_v \Lambda \left[P_v \rho P_v \right] P_v \\
&= \sum_{P_v \in \mathcal{P}_n} f_{vv} P_v \rho P_v.
\end{aligned} \tag{38}
$$

We apply PTA to the spectral quantum process tomography elaborated in Sec. II D to extract SPAM free spectral of dynamical map for twirled Pauli channel. Under the PTA, the generalized signal functions for non-Markovian processes, defined in Eqs. (14) and (15), should read

$$
\begin{aligned}
g'_{t_n}(k) = &\frac{1}{2^n} \sum_{\mu=1}^{N} \text{Tr} \Big[P_\mu \mathcal{N}_m \circ \tilde{\Lambda}_n \\
&\circ \left(M_\mu \circ \mathcal{N}_m \circ \tilde{\Lambda}_n \right)^{k-1} \circ \mathcal{N}_p \left(P_\mu \right) \Big]
\end{aligned} \tag{39}
$$

and

$$
\begin{aligned}
g''_{t_n}(k) = &\frac{1}{2^n} \sum_{\mu=1}^{N} \text{Tr} \Big[P_\mu \mathcal{N}_m \circ M'_\mu \circ \tilde{\Lambda}_n \\
&\circ \left(M'_\mu \circ M'_\mu \circ \tilde{\Lambda}_n \right)^{k-1} \circ \mathcal{N}_p \left(P_\mu \right) \Big]
\end{aligned} \tag{40}
$$

where $\tilde{\Lambda}_n$ is the twirled Pauli channel for Λ_n. As proved in Appendix A, the projective measurement-based spectral tomographic technique introduced in Sec. II D is compatible with PTA. Hence, from $g'_{t_n}(k)$ and $g''_{t_n}(k)$, one obtains the spectrum for the twirled Pauli channel $\tilde{\Lambda}_n$.

Now, we clarify a few technical subtleties. First, we do not explicitly account for any gate errors incurred during the twirling approximations. As indicated in Eqs. (39)–(40), the construction of kth signals requires the Pauli twirling approximation k times. From Eq. (38), it is clear that every twirling operation involves tensor products of Pauli operations on each qubit, and these Pauli operations can be implemented very efficiently (i.e., over a much shorter period than the duration for each identity gate we investigate for noise characterization). For many high-quality quantum hardwares, the environment-induced decoherence should be just weak perturbation, and the quantum dynamics should be mainly driven by the strong pulse during the execution of the single-qubit operations. Hence, the coherent errors should dominate for these simple gates. Under the PTA, these coherent errors are turned into additional incoherent errors and are typically taken to be Markovian. For simplicity, we ignore these additional errors in the subsequent discussions of non-Markovianity.

A major focus of this work is to propose a SPAM error-free approach to quantify the degree of non-Markovianity for the noises surrounding a quantum device composed of qubits. Obviously, analysis on the PTA channel $\tilde{\Lambda}_n$ only yields a skewed spectral information of the original quantum process Λ_n, and poses challenges for an accurate non-Markovian quantification. We should address this problem in two steps. First, we stress that the RHP measure based on $\tilde{\Lambda}_n$ is still a faithful witness of non-Markovianity for Λ_n. Note, if the original quantum process is CP divisible for all time t then its PTA must obey the CP divisibility too. Hence, a nonzero RHP measure for $\tilde{\Lambda}_n$ clearly signals a violation of CP divisibility of Λ_n for some t_n. The second step is to recover as accurate a quantification as possible. Details are deferred to the following subsection.

B. Optimal twirling basis for non-Markovian quantification

We now discuss the idea of an optimal basis for getting a more accurate non-Markovian quantification (based on the RHP measure). For simplicity, we illustrate the idea of PTA in an optimal basis with a single qubit. First, we introduce a new basis P'_v by applying some unitary transformation to the standard Pauli basis,

$$
P'_v \in \left\{ I, UP_x U^\dagger, UP_y U^\dagger, UP_z U^\dagger \right\}, \tag{41}
$$

where $U \equiv U(\theta_1, \theta_2, \theta_3) = \mathcal{R}_{\hat{z}}(\theta_1) \mathcal{R}_{\hat{y}}(\theta_2) \mathcal{R}_{\hat{z}}(\theta_3)$. A PTA channel in the new basis reads

$$
\tilde{\Lambda}(\rho) = \sum_{P'_v \in \mathcal{P}_n} f'_{vv} P'_v \rho P'_v. \tag{42}
$$

We propose to identify an optimal Pauli basis, induced by $U(\theta_1, \theta_2, \theta_3)$, such that the corresponding PTA channel $\tilde{\Lambda}$ gives a maximized RHP measure. The rationale for this maximization is now elucidated. A non-CPTP map $\Lambda(t + \epsilon, t) \approx I + \mathcal{L}(t)\epsilon$ at time t may give a nonphysical density matrix (i.e., nonpositive semidefinite) when it is applied to $\Phi\rangle\langle\Phi|$, a maximally entangled bipartite system. The operator $\mathcal{L}(t)$ is the generator for $\Lambda(t + \epsilon, t)$. We now draw attention to a mathematical fact

$$
\sum_j |d_j| \le \sum_j \sigma_j, \tag{43}
$$

where $|d_j|$ and σ_j are the jth absolute eigenvalue and singular value for the density matrix ρ, respectively, and are sorted in a nonincreasing order. An immediate consequence of this inequality is that $\tilde{\mathbf{g}}(t)$, the RHP measure for $\tilde{\Lambda}(t + \epsilon, t)$, is always upper bounded by $\mathbf{g}(t)$, the RHP measure for $\Lambda(t + \epsilon, t)$. With any given Pauli basis, an estimate

on the accumulated errors is

$$
\begin{aligned}
\mathbf{g}(t) &= \lim_{\epsilon \to 0^+} \frac{\| [I + (\mathcal{L}_t \otimes I) \epsilon] |\Phi\rangle\langle\Phi|\|_1 - 1}{\epsilon} \\
&= \lim_{\epsilon \to 0^+} \frac{\| \left[I + \left(\tilde{\mathcal{L}}_t + \delta\mathcal{L}_t \otimes I \right) \epsilon \right] |\Phi\rangle\langle\Phi|\|_1 - 1}{\epsilon} \\
&\leq \tilde{\mathbf{g}}(t) + \| (\delta\mathcal{L}_t \otimes I) |\Phi\rangle\langle\Phi|\|_1,
\end{aligned} \tag{44}
$$

where $\delta\mathcal{L}_t = \mathcal{L}_t - \tilde{\mathcal{L}}_t$. From the penultimate line to the last line in Eq. (44), we use the triangular inequality. Clearly, an optimal basis that trying to saturate the upper bound in Eq. (43) would also largely minimize the errors present in Eq. (44).

V. RESULTS

We illustrate how to use STTM to quantify non-Markovianity and noise power spectrum for Pauli and non-Pauli channels through numerical experiments.

A. STTM spectroscopy of Pauli channel

We first consider a one-qubit pure phasing model, which is a Pauli channel. The Hamiltonian reads $H_s = \omega_s \sigma^z$ and $H_{sb} = B^z(t)\sigma^z$. The noise $B^z(t)$, a Gaussian process, possesses the statistical moments: $\langle B^z(t) \rangle = 0$ and $C_{zz}(t - t') = \langle B^z(t)B^z(t') \rangle = \lambda e^{-|t-t'|} \cos[\omega_c(t - t')]$. For these cosine functions modulated by an exponentially decaying envelope, the corresponding power spectrum assumes a Lorentzian profile.

The pure-dephasing dynamical maps are given by

$$
\Lambda_n = \begin{bmatrix} 1 & 0 & 0 & 0 \\ 0 & e^{-\Upsilon(t_n)+i2\omega_s t} & 0 & 0 \\ 0 & 0 & e^{-\Upsilon(t_n)-i2\omega_s t} & 0 \\ 0 & 0 & 0 & 1 \end{bmatrix}, \tag{45}
$$

with

$$
\Upsilon(t) = \frac{4}{\pi} \int_0^\infty d\omega \frac{S(\omega)}{\omega^2} [1 - \cos(\omega t)]. \tag{46}
$$

Note that these dynamical maps satisfy $\rho(t_n) = \Lambda_n \rho(0)$ as required. It is straightforward to verify that these maps are not divisible, i.e. $\Lambda_{n+m} \neq \Lambda_n \Lambda_m$, and the dynamics is clearly non-Markovian. The spectrum of the dynamical map may be read off the diagonal in Eq. (45) as $\{e^{-\Upsilon(t_n)+i2\omega_s t}, e^{-\Upsilon(t_n)-i2\omega_s t}, 1\}$.

We complicate the simulation of this one-qubit pure-dephasing model by adding random noises during the state preparations and measurements. We then extract the SPAM error-free eigenvalues of the dynamical maps with the SQPT and construct the STTM according to Eq. (17a). In Fig. 3(a) we plot $|\tau_n^\alpha|$ at different times.

Since, for the pure-dephasing model, $|\tau_n^1| = |\tau_n^2|$, $|\tau_1^3| = 1$, and $|\tau_n^3| = 0$ for $n > 1$, we present only the result for $|\tau_n^1|$. As illustrated in Fig. 3(a), more than one TTM have non-negligible norm. This observation confirms that the non-Markovianity of a dynamical process is directly correlated with $|\tau_n^\alpha|$ distribution. Furthermore, it is clear that the higher order $|\tau_n^\alpha|$ are increasingly suppressed. This trend justifies an earlier claim that we should be able to truncate Eq. (17b) to only the first few STTMs with nontrivial norms for dynamical predictions based on Eq. (17a). In Fig. 3(b), we plot the spectrum of the dynamical map as a function of time. Since $|\lambda_n^1| = |\lambda_n^2|$ and $|\lambda_n^3| = 1$, we only present the result for $|\lambda_n^1|$. The curve with black squares is the exact result $e^{-\Upsilon(t)}$, which requires explicitly evaluating the integral in Eq. (46) at every time point. The other curves are results obtained by using different numbers of STTMs in the way prescribed by Eq. (17a) to predict quantum dynamical evolution. In this case, we consider using the first $n = 1, 4, 8$ STTMs, respectively. Accurate results are obtained for the entire simulation duration when a sufficient number ($n = 8$) of STTMs are taken into account.
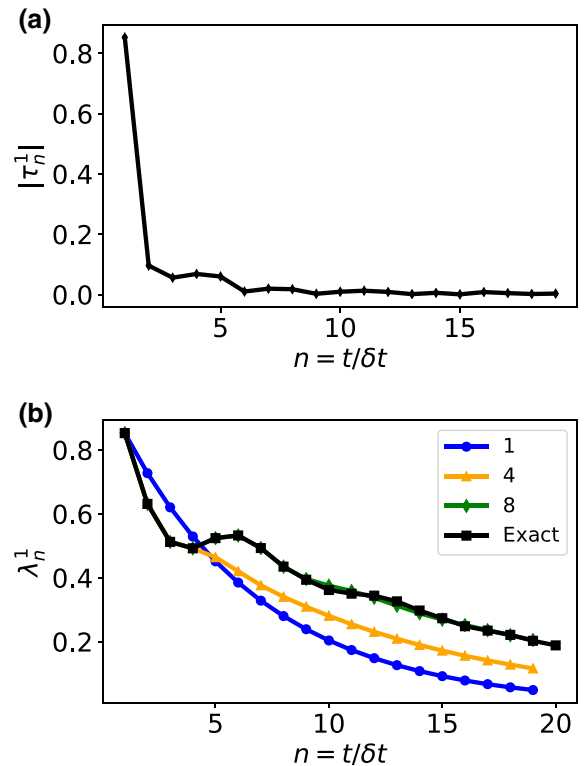

FIG. 3. STTM for a single-qubit pure-dephasing model. (a) Absolute value distribution of the STTM, τ_n^α over time. (b) Dynamical map spectral predictions by STTM. The model parameters are $H_{sb} = B^z(t)\sigma^z$, $C_{zz}(0) = \lambda = 4$, and $\delta t = 0.2$.
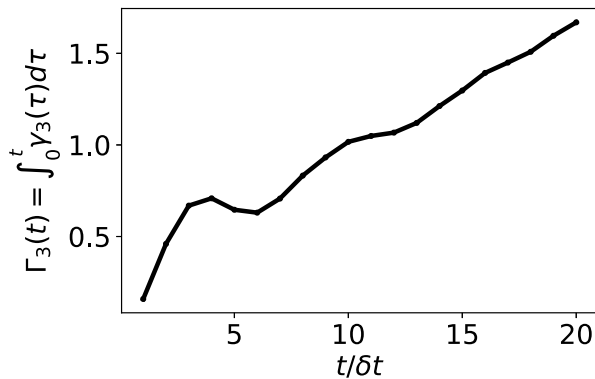
FIG. 4.   Non-Markovianity of single-qubit pure-dephasing model. The model parameters are $H_s = 0.1\sigma_z$, $H_{sb} = B^z(t)\sigma^z$, $C_{zz}(0) = \lambda = 4$, and $\delta t = 0.2$.

Next we analyze the non-Markovianity of the dynamical process by plotting $\Gamma_\alpha(t)$, the integral of decoherence rate at different times [as defined in Eq. (25)] in Fig. 4. As discussed in the previous section, the RHP measure for non-Markovianity implies that the nonmonotonic trending behavior of $\Gamma_\alpha(t)$ is an absolute signature of non-Markovian dynamics. This nonmonotonicity is indeed manifested around t_4 in Fig. 4. We show only $\Gamma_3(t)$, since $\Gamma_1(t) = \Gamma_2(t) = 0$. This is an encouraging indication that STTM may facilitate the implementation of the RHP measure in an experiment.

A critical role of a quantum noise spectroscopy is to determine the noise power spectrum. Since a spectrum is essentially the Fourier transform of the corresponding correlation function, we are content if we may easily obtain noise correlation functions in experiments. We consider the case of weakly coupled noise where the approximation $\mathcal{K}(t) \approx \mathcal{K}_2(t)$ is valid. We use Eq. (36) to infer the targeted correlation function. In Fig. 5, we plot the numerically recovered correlation function based on the TTM data, and it agrees well with the theoretical correlation function that the random noise $B^z(t)$ must satisfy in our numerical experiment.

Besides the pure-dephasing channel, other well-known noisy dynamics such as depolarization channel and amplitude damping channel in a quantum circuit can all be rigorously analyzed with the STTM (which fully characterizes non-Markovian dynamics of any Pauli channels). In Appendix C, we present another simulation experiment, considering the depolarization channel. While the depolarization process is clearly a Pauli channel, the single-qubit amplitude damping channel deserves some clarifications. We note the amplitude damping channel can be described by the Kraus matrix,

$$E_1 = \begin{pmatrix} 1 & 0 \\ 0 & \sqrt{1-p} \end{pmatrix}, E_2 = \begin{pmatrix} 0 & \sqrt{p} \\ 0 & 0 \end{pmatrix}. \quad (47)$$
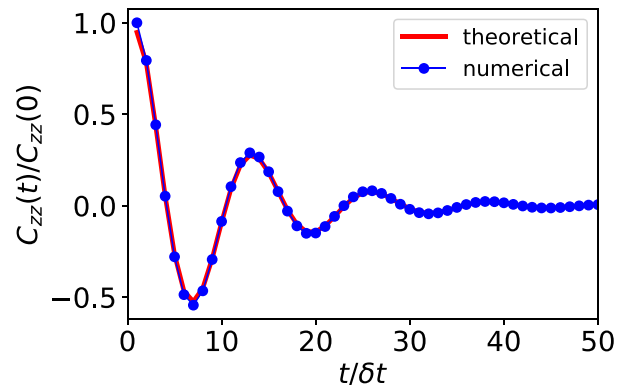

FIG. 5.   TTM noise spectroscopy of pure-dephasing model. The numerically extracted correlation function (from the memory kernel) matches well with the theoretical result $C_{zz}(t) = \langle B^z(t)B^z(0)\rangle$. Model parameters are $H_s = 0.02\sigma_z$, $C_{xx}(0) = 0.04$, and $dt = 0.1$.

It can be expressed by Pauli matrices

$$\Lambda(\rho) = \sum_{P_v \in \mathcal{P}_n} f_{vv'} P_v \rho P_{v'} \quad (48)$$

with $f_{00} = (1 + \sqrt{1-p}/2)^2$, $f_{11} = f_{22} = p/4$, $f_{33} = (1 - \sqrt{1-p}/2)^2$, $f_{03} = f_{30} = p/4$, $f_{21} = -f_{12} = -p/4i$. It is clear that Eq. (48) is not a Pauli channel. However, according to Eq. (4), the resulting Pauli transfer matrix is diagonal with $R_{11} = \sqrt{1-p}$, $R_{22} = \sqrt{1-p}$, $R_{33} = 1-p$, which is the same as the results after a PTA. This is why STTM can accurately characterize non-Markovianity of an amplitude damping channel.

B. STTM spectroscopy beyond Pauli channel

We next illustrate how well STTM may characterize a non-Pauli channel. For simplicity, let us consider a general Hamiltonian for an idling qubit in a quantum circuit,

$$H_{sb} = B^x(t)\sigma^x + B^y(t)\sigma^y, \quad (49)$$

where $B^x(t)$, $B^y(t)$ are assumed to be correlated Gaussian noises, and satisfy the statistical moments: $\langle B^x(t)\rangle = 0$, $\langle B^y(t)\rangle = 0$ with $C_{xx}(t - t') = \langle B^x(t)B^x(t')\rangle = \lambda_1 e^{-|t-t'|} \cos[\omega_c(t - t')]$, $C_{yy}(t - t') = \langle B^y(t)B^y(t')\rangle = \lambda_2 e^{-|t-t'|} \cos[\omega_c(t - t')]$, and $C_{xy}(t - t') = \langle B^x(t)B^y(t')\rangle = \lambda_3 e^{-|t-t'|} \cos[\omega_c(t - t')]$.

Firstly, we apply the PTA in the computational basis to effectively enforce a Pauli channel and conduct experiments to acquire STTM. In Fig. 6(a), we compare Γ_t, estimated under different means, for this one-qubit system. The red squares present that the rigorous Γ_t that could be numerically determined without resorting to PTA for this simple model. The blue lines give Γ_t after PTA in the computational basis. In this case, we reconstruct Γ_t (blue line)

from STTM dataset via Eqs. (17b) and (25). Clearly, the approximated result (blue lines) deviates significantly from the exact one (red squares).

Next, we consider the method discussed in Sec. IV B to search for an optimal twirling basis in order to better represent the correct dynamics with a Pauli channel. In Fig. 6(b), we present Γ_t (green lines) deduced from STTM based on this optimal basis. As clearly shown, the approximated results under optimal basis agree well with the original one. In other words, the non-Markovianity of a non-Pauli channel can be maximally recovered with an optimal basis. Note that we purposely choose a rather challenging scenario (in Fig. 6) to illustrate the effectiveness of doing Pauli twirling in an optimal basis to gauge the non-Markovianity of a noisy quantum process. In Appendix D, we further discuss realistic scenarios in which the Pauli twirling conducted under the original computational basis can still provide meaningful characterization of the non-Markovianity.
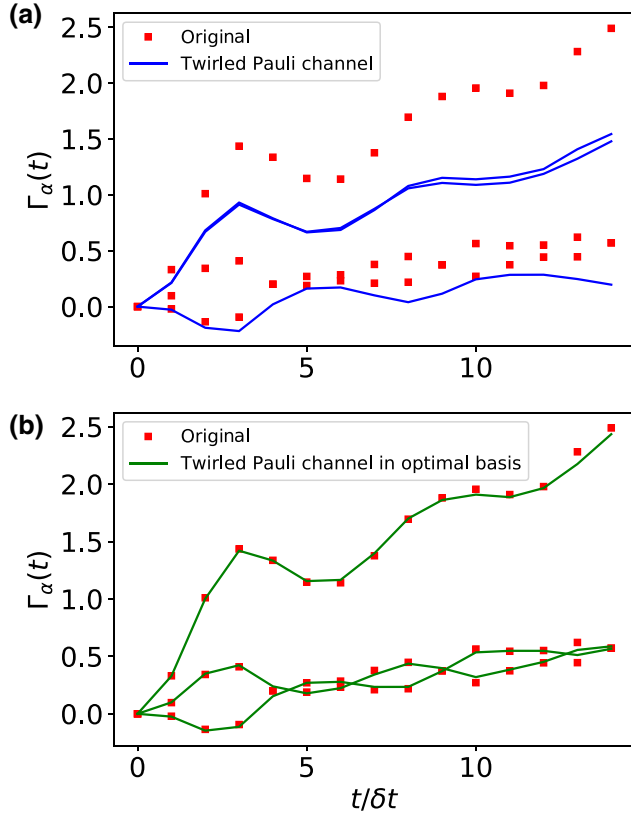

FIG. 6. Non-Markovianity of non-Pauli channel. (a) The non-Markovanity of original non-Pauli channel (red squares) and non-Markovanity of Pauli channel by PTA in standard basis (blue lines). (b) The non-Markovanity of original non-Pauli channel (red squares) and non-Markovanity of Pauli channel by PTA in optimal basis (green lines). The model parameters are $H_{sb} = B^x(t)\sigma^x + B^y(t)\sigma^y$, $C_{xx}(0) = \lambda_1 = 5, C_{yy}(0) = \lambda_2 = 5, C_{xy}(0) = \lambda_3 = 3$, and $\delta t = 0.2$.

VI. CONCLUSION

In this work, we propose STTM for characterizing the SPAM error-free spectrum of non-Markovian Pauli channels. Our proposed protocol relies on SQPT to extract spectral information of a dynamical map, then the standard TTM relations can be alternatively cast into spectral versions for Pauli channels. As illustrated in this work, the STTM approach can accurately capture every aspect of a non-Markovian Pauli channel. With access to the STTM data, it is possible to (1) assess the non-Markovianity, and (2) reconstruct the noise power spectrum. As argued earlier, Pauli channels (and generalized cases including amplitude damping channels with a diagonal R submatrix inside the Pauli transfer matrix) represent most popular noise and error models for quantum circuits due to various physical motivations. Beyond Pauli channels, we also propose to identify an optimal basis to apply Pauli twirling approximation and collect the STTM data in order to better characterize the dynamical process of interests.

While SQPT under PTA captures only partial information of a general quantum channel, the reconstructed STTM still encodes useful information, such as giving an estimate on the degrees of non-Markovianity of a noisy process. As we continuously improve the quality of quantum devices, it becomes more crucial to have a simple approach to quantify non-Markovianity in a high-precision manner, for instance, complete removal of SPAM errors. Probing this subtle aspect of a noisy process will certainly help to design better quantum hardwares.

We acknowledge that STTM is not as scalable a protocol as the randomized benchmarking. However, it does not imply STTM is not useful for noise characterization of large-scale quantum devices. We can adopt a divide-and-conquer approach to divide a large device into small parts and analyze the local noises in a much more economical fashion, see, for example, Ref. [37]. Particularly, we note that STTM is not necessarily consuming more resources (to conduct the data-acquisition experiments) than standard QPT. Yet, one gets SPAM error-free estimates on the spectrum of dynamical processes, which usually requires a SPAM-resistant tomographic technique that consumes even way more resources. Hence, we argue that STTM is currently the method of choice that balances the trade-off between resource consumption and level of characterization if one desires to probe non-Markovianity of a noisy process in a quantum circuit.

Finally, STTM could be further optimized by adopting more sophisticated methods to reduce the experimental costs of performing QPTs such as the compressed sensing and other approaches. Being able to conduct careful analysis on clusters of a small number of neighboring qubits in a connectivity-limited hardware architecture is among the most promising applications of STTM in the NISQ era.

APPENDIX A: SIGNAL FUNCTIONS FOR NON-MARKOVIAN CHANNEL

We propose a protocol to construct a dynamical map $(\Lambda_n)^k$, which is the k-times composition of a non-Markovian Pauli channel Λ_n at time $t = t_n$. The corresponding signal function at time t_n reads

$$g'_{t_n}(k) = \frac{1}{2^n} \sum_{\mu=1}^{N} \text{Tr}\left[P_\mu \mathcal{N}_m \circ \Lambda_n \circ \left(M_\mu \circ \mathcal{N}_m \circ \Lambda_n \right)^{k-1} \right.$$
$$\left. \circ \mathcal{N}_p \left(P_\mu \right) \right], \tag{A1}$$

where

$$M_\mu[\rho] = P_+ \rho P_+ + P_- \rho P_-. \tag{A2}$$

A Pauli matrix can be decomposed as follows: $P_\mu = \sum_+ |\mu_+\rangle \langle \mu_+| - \sum_- |\mu_-\rangle \langle \mu_-| = \sum_+ P_+ - \sum_- P_-$, where $|\mu_+\rangle$ denote eigenvectors with a positive eigenvalue, and $|\mu_-\rangle$ denote eigenvectors with a negative eigenvalue. Because $\text{Tr}[P_\mu \Lambda_n(\sum_+ P_+)] + \text{Tr}[P_\mu \Lambda_n(\sum_- P_-)] = 0$, we deduce that $\text{Tr}[P_\mu \Lambda_n(P_\mu)] = 2\text{Tr}[P_\mu \Lambda_n(\sum_+ P_+)]$. Thus, SQPT can be attained by preparing $d/2$ initial states for each P_μ.

$$g'_{t_n}(k) = \frac{1}{2^{(n-1)}} \sum_{\mu=1}^{N} \text{Tr}\left[P_\mu \mathcal{N}_m \circ \Lambda_n \circ \left(M_\mu \circ \mathcal{N}_m \circ \Lambda_n \right)^{k-1} \right.$$
$$\left. \circ \mathcal{N}_p \left(P_+ \right) \right]$$
$$= \sum_{\mu=1}^{N} R_{\mu\mu}(k). \tag{A3}$$

For Pauli channel, the R matrix is clearly diagonal. The construction of k-times composition of a dynamical map is simply related to construction of kth power of the diagonal matrix $R_{\mu\mu}(1)$. For simplicity, we outline the proof for the single-qubit case without considering SPAM errors. In particular, it is to verify the following relation for $g_{t_n}(1)$:

$$R_{\mu\mu}(1) = \text{Tr}[P_\mu \Lambda_n(P_+)]$$
$$= (W_1 - W_2), \tag{A4}$$

where $\langle \mu_+ | \Lambda_n (P_+) | \mu_+\rangle = W_1$ and $\langle \mu_- | \Lambda_n (P_+) | \mu_-\rangle = W_2$. To facilitate the following discussion, we also introduce $\langle \mu_+ | \Lambda_n (P_-) | \mu_+\rangle = W_3$ and $\langle \mu_- | \Lambda_n (P_-) | \mu_-\rangle = W_4$. Recall the definition of M_μ in Eq. (A2), then it is also straightforward to establish the following relations for $g_{t_n}(2)$:

$$R_{\mu\mu}(2) = \text{Tr}[P_\mu \Lambda_n \circ M_\mu \circ \Lambda_n(P_+)]$$
$$= W_1 \times W_1 + W_3 \times W_2 - W_2 \times W_1 - W_4 \times W_2. \tag{A5}$$

Again, since $\text{Tr}[P_\mu \Lambda_n(P_+)] + \text{Tr}[P_\mu \Lambda_n(P_-)] = 0$, we have $W_1 - W_2 = W_4 - W_3$ and

$$R_{\mu\mu}(2) = W_1 \times W_1 + W_2 \times W_2 - W_2 \times W_1 - W_1 \times W_2$$
$$= R_{\mu\mu}(1)^2. \tag{A6}$$

If we repeat the analysis for the elements of $g_{t_n}(k)$ for $k = 1, 2, \ldots, K$, then we should attain

$$R_{\mu\mu}(k) = R_{\mu\mu}(1)^k. \tag{A7}$$

So far, we discuss how the construction of k multiplicative of a dynamical map can be realized by projective measurements. However, as this protocol relies on making k measurements, the results are also affected by the accompanied measurement errors,

$$g'_{t_n}(k) = \frac{1}{2^n} \sum_{\mu=1}^{N} \text{Tr}\left[P_\mu \left(\mathcal{N}_m \circ \Lambda_n \right)^k \circ \mathcal{N}_p \left(P_\mu \right) \right]$$
$$= \text{Tr}\left[(R_{\text{meas}} R)^k R_{\text{prep}} \right]$$
$$= \text{Tr}\left[A_P D^k \right] = \sum_{j=1}^{N} A_j \left(m_j \lambda_j \right)^k \tag{A8}$$

In order to remove these measurement errors, we propose a supplementary protocol in which the original single projective measurement is replaced by double measurements. Going through the same analysis laid out for the single-measurement protocol described above, the double-measurement protocol leads to the following signal function:

$$g''_{t_n}(k) = \frac{1}{2^n} \sum_{\mu=1}^{N} \text{Tr}\left[P_\mu \left(\mathcal{N}_m \circ \mathcal{N}_m \circ \Lambda_{ti} \right)^k \circ \mathcal{N}_p \left(P_\mu \right) \right]$$
$$= \text{Tr}\left[(R_{\text{meas}} R_{\text{meas}} R)^k R_{\text{prep}} \right]$$
$$= \text{Tr}\left[A_P D^k \right] = \sum_{j=1}^{N} A_j \left(m_j^2 \lambda_j \right)^k. \tag{A9}$$

As shown in Eq. (16) of the main text, one can easily recover SPAM-error-free eigenvalues of the Pauli channel by extracting the spectral information from $g'_{t_n}(k)$ and $g''_{t_n}(k)$.

APPENDIX B: VALIDITY REGIME OF STTM

To quantify the non-Markovianity of a noisy process, the STTM method proposes to insert projective measurements between k sequences of n time-step free evolution of a quantum system in the presence of the noise to effectively realize a series of Markovian process Λ_n^k using the technique of the spectral quantum spectrum tomography, see Eqs. (14)–(15). However, the projective measurement may yield correlations a system-dependent environmental state [30], which compromises the goal of constructing an effective Markovian channel. As a result, STTM (as given) holds in the following regimes.

(1) The environment can be modeled as a classical noise source. Hence, the projective measurement will not yield any system-environment correlation. According to previous studies, the decoherence of many quantum systems (for making qubits) may be explained with semiclassical models in which the environmental influence is driven by fluctuating classical noises [38–44]. For examples, in superconducting qubit systems, fluctuating electric charges and spin centers produce classical noise [38,39]; the inhomogeneous broadening of the ground state by the trap magnetic field is identified as the principal mechanism for decoherence [41,42].

(2) Non-Markovian channel with weak system-environment coupling strength and short correlation times for the environmental degrees of freedom according to a recent study [30]. For the case beyond this regime, we can refer to research [30] to conduct more accurate analysis by introducing an additional correction term in the transfer tensor map.

In the main text, we discuss all the theorems that implicitly satisfying the conditions outlined above. Particularly, the simulation experiments are all conducted with classical noise models.

APPENDIX C: NON-MARKOVIAN DEPOLARIZATION CHANNEL

We illustrate the ability of STTM to characterize a non-Markovian depolarization channel, which is another common decoherence model for qubits [45,46]. For simplicity, let us consider a general Hamiltonian for an idling qubit in a quantum circuit,

$$H_{sb} = B^x(t)\sigma^x + B^y(t)\sigma^y + B^z(t)\sigma^z, \qquad (C1)$$

where $B^x(t), B^y(t), B^z(t)$ are assumed to be correlated Gaussian noises, and satisfy the statistical moments: $\langle B^x(t) \rangle = 0, \langle B^y(t) \rangle = 0, \langle B^z(t) \rangle = 0.$ $C_{xx}(t - t') = C_{yy}(t - t') = C_{zz}(t - t') = \lambda e^{-|t-t'|} \cos[\omega_c(t - t')]$. All cross correlations, such as C_{xy} etc., vanish. Hence, these noises
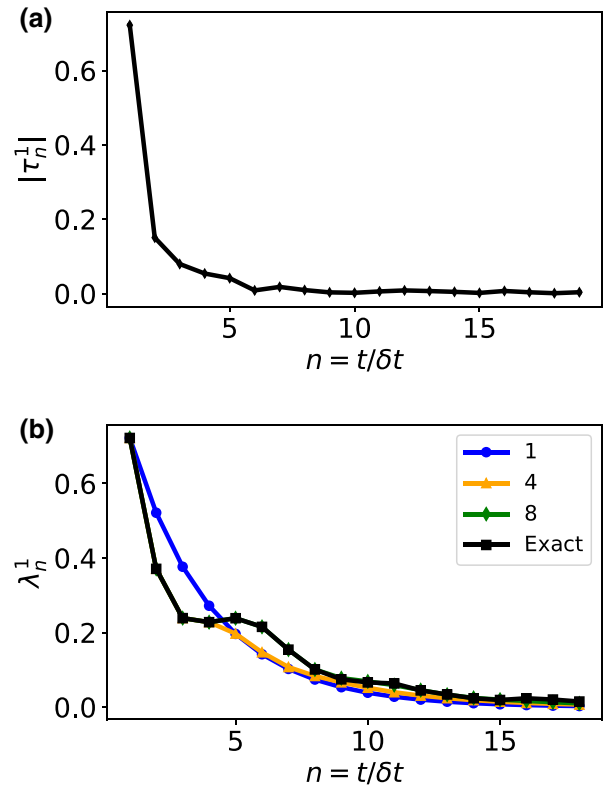

FIG. 7. STTM for a single-qubit depolarization model. (a) Absolute value distribution of the STTM, τ_n^α over time. (b) Dynamical map spectral predictions by STTM. The model parameters are $\lambda = 4, \delta t = 0.2$.

effectively provide a non-Markovian depolarization channel for the qubit.

In Fig. 7(a) we plot $|\tau_n^\alpha|$ at different times. Since, for the depolarization model, $|\tau_n^1| = |\tau_n^2| = |\tau_n^3|$, we present only the result for $|\tau_n^1|$. As illustrated in Fig. 7(a), more than one TTMs have non-negligible norm. This observation confirms that the non-Markovianity of a dynamical process is directly correlated with the $|\tau_n^\alpha|$ distribution. Furthermore, it is clear that the higher order $|\tau_n^\alpha|$ are increasingly suppressed. This trend justifies an earlier claim that we should be able to truncate Eq. (17b) to only the first few STTMs with nontrivial norms for the dynamical predictions based on Eq. (17a). In Fig. 7(b), we plot the spectrum of the dynamical map as a function of time. Since $|\lambda_n^1| = |\lambda_n^2| = |\lambda_n^3|$, we present only the result for $|\lambda_n^1|$. The curve with black squares is the exact result $e^{-\Upsilon(t)}$, which entails an explicit evaluation of the integral in Eq. (46) at every time point. The other curves are results obtained by using different numbers of STTMs in the way prescribed by Eq. (17a) to predict the quantum dynamical evolution. In this case, we use the first $n = 1, 4, 8$ STTMs, respectively, to produce the corresponding results in the figure. Accurate results are obtained for the entire simulation duration

when a sufficient number ($n = 8$) of STTMs are taken into account.

APPENDIX D: PAULI TWIRLING APPROXIMATION

Even without the basis optimization, which means conducting Pauli twirling in original computational basis, we can still capture the trend of non-Markovianity of noisy quantum processes. We further illustrate this point with a detailed example. In this section, we investigate the noise channel $H_{sb} = B^x(t)\sigma^x + B^y(t)\sigma^y + B^z(t)\sigma^z$, where $\langle B_z(t)B_z(t')\rangle \propto \gamma_z$ denoting the Pauli component of noise channel, $\langle B_x(t)B_x(t')\rangle \propto \gamma_x$, $\langle B_y(t)B_y(t')\rangle \propto \gamma_y$, $\langle B_x(t)B_y(t')\rangle \propto \gamma_{x,y}$ denoting the non-Pauli components of noise channel.

As shown in Fig. 8, the non-Markovianity for the twirled Pauli channel (blue square) perfectly agrees with the original channel (red dot) for the Pauli channel when $\gamma_{x,y} = 0$. With the increase of $\gamma_{x,y}$, the non-Pauli channel components become more relevant to affecting the qubits. As a result, the non-Markovianity for the twirled Pauli channel (blue squares) deviates from that of the original channel (red dots). However, the twirled Pauli channel in an optimized basis can satisfactorily recover the non-Markovianity (green triangles). Furthermore, as manifested in Fig. 8, the Pauli twirling approximation maintains the right order of non-Markovianity across the entire range of possible ratios of $\gamma_{x,y}/\gamma_z$. In short, simple Pauli twirled results can still be used to infer which noise setting is more non-Markovian when dealing with a family of highly similar noisy environments. For instance, this could be the scenario when we characterize multiple qubits in a single chip or ion trap etc.
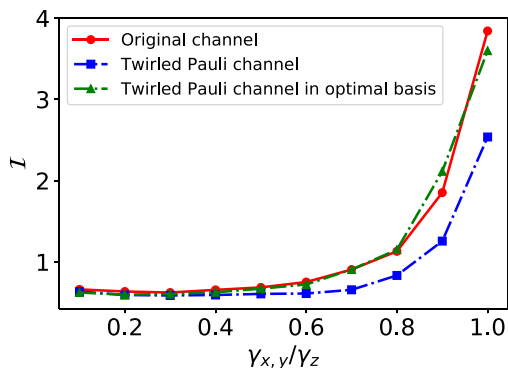
FIG. 8.   Non-Markovanity of non-Pauli channel with the growing up of non-Pauli components. The non-Markovanity of original non-Pauli channel (red dots) and non-Markovanity of Pauli channel by PTA in standard basis (blue squares). The non-Markovanity of Pauli channel by PTA in optimal basis (green triangles).

APPENDIX E: ANALYSIS ON THE TIME DISCRETIZATION

The STTM method proposed in the main text is performed in discretized form at equidistant time intervals, i.e. $t_k = k\delta t$. The time step size δt decides the degree of deviation of time discretization from the theoretically considered infinitesimal time step.

We numerically study the convergence of non-Markovianity dictated by the time discretization for the pure-dephasing model. In Fig. 9(a) we show $\Gamma_3(t)$ of different time-step size changing from $\delta t = 0.025$ to $\delta t = 0.8$ with total time length $T = 4$. In Fig. 9(b) we directly present the non-Markovianity calculated by $I = \sum_\alpha \int_{\gamma_\alpha(t)<0} -\gamma_\alpha(t)dt$ of different time-step size changing from $\delta t = 0.025$ to $\delta t = 0.8$. We can see that the precision of the non-Markovianity characterization is acceptable for a wide region of time-step size $\delta t/T \in (0, 0.1)$. When conducting an experiment on quantum device, the time-step size often constrained by the hardware design. In other words, the minimum time-step size is roughly equal to the time required to conduct a single quantum gate. According to the recent researches of non-Markovian noise on the IBM quantum devices [20,47], the time length of
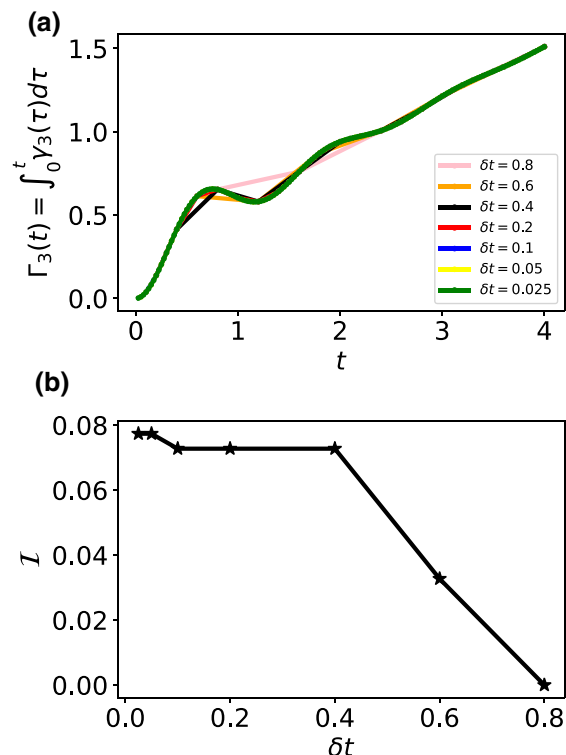
FIG. 9.   Non-Markovianity of different time-step size. (a) $\Gamma_3(t)$ of different time-step size changing from $\delta t = 0.025$ to $\delta t = 0.8$ with total time length $T = 4$. (b) Non-Markovianity calculated by $I = \sum_\alpha \int_{\gamma_\alpha(t)<0} -\gamma_\alpha(t)dt$ of different time-step size changing from $\delta t = 0.025$ to $\delta t = 0.8$.

non-Markovian memory kernel involves 300–800 numbers of pulse [$\delta t/T \in (0.001, 0.003)$], which satisfies the precision requirement of time-step size of non-Markovianity characterization.

———————

[1] John Preskill, Quantum computing in the NISQ era and beyond, Quantum **2,** 79 (2018).

[2] Robin Blume-Kohout, John King Gamble, Erik Nielsen, Kenneth Rudinger, Jonathan Mizrahi, Kevin Fortier, and Peter Maunz, Demonstration of qubit operations below a rigorous fault tolerance threshold with gate set tomography, Nat. Commun. **8,** 1 (2017).

[3] Daniel Greenbaum, Introduction to quantum gate set tomography, (2015), arXiv preprint ArXiv:1509.02921.

[4] Isaac L. Chuang and M. A. Nielsen, Prescription for experimental determination of the dynamics of a quantum black box, J. Mod. Opt. **44,** 2455 (1997).

[5] J. F. Poyatos, J. I. Cirac, and P. Zoller, Complete Characterization of a Quantum Process: The Two-Bit Quantum Gate, Phys. Rev. Lett. **78,** 390 (1997).

[6] M. A. Nielsen and I. L. Chuang, *Quantum Computation and Quantum Information* (Cambridge University Press, Cambridge, England, 2000).

[7] Emanuel Knill, Dietrich Leibfried, Rolf Reichle, Joe Britton, R. Brad Blakestad, John D. Jost, Chris Langer, Roee Ozeri, Signe Seidelin, and David J. Wineland, Randomized benchmarking of quantum gates, Phys. Rev. A **77,** 012307 (2008).

[8] Easwar Magesan, Jay M Gambetta, and Joseph Emerson, Scalable and Robust Randomized Benchmarking of Quantum Processes, Phys. Rev. Lett. **106,** 180504 (2011).

[9] Shelby Kimmel, Marcus P. da Silva, Colm A. Ryan, Blake R. Johnson, and Thomas Ohki, Robust Extraction of Tomographic Information via Randomized Benchmarking, Phys. Rev. X **4,** 011050 (2014).

[10] Joseph Emerson, Robert Alicki, and Karol Życzkowski, Scalable noise estimation with random unitary operators, J. Opt. B: Quantum Semiclassical Opt. **7,** S347 (2005).

[11] Jun Zhang and Mohan Sarovar, Quantum Hamiltonian Identification From Measurement Time Traces, Phys. Rev. Lett. **113,** 080401 (2014).

[12] Jianwei Wang, Stefano Paesani, Raffaele Santagati, Sebastian Knauer, Antonio A. Gentile, Nathan Wiebe, Maurangelo Petruzzella, Jeremy L. O'Brien, John G. Rarity, and Anthony Laing, *et al.*, Experimental quantum Hamiltonian learning, Nat. Phys. **13,** 551 (2017).

[13] Akira Sone and Paola Cappellaro, Hamiltonian identifiability assisted by a single-probe measurement, Phys. Rev. A **95,** 022335 (2017).

[14] Eyal Bairey, Itai Arad, and Netanel H. Lindner, Learning a Local Hamiltonian from Local Measurements, Phys. Rev. Lett. **122,** 020504 (2019).

[15] R. J. Schoelkopf, A. A. Clerk, S. M. Girvin, K. W. Lehnert, and M. H. Devoret, *NATO Science Series in Mathematics*, edited by Yu. V. Nazarov, (Kluwer, Dordrecht, 2003).

[16] Lara Faoro and Lorenza Viola, Dynamical Suppression of $1/f$ Noise Processes in Qubit Systems, Phys. Rev. Lett. **92,** 117905 (2004).

[17] Kevin C. Young and K. Birgitta Whaley, Qubits as spectrometers of dephasing noise, Phys. Rev. A **86,** 012314 (2012).

[18] Jonas Bylander, Simon Gustavsson, Fei Yan, Fumiki Yoshihara, Khalil Harrabi, George Fitch, David G Cory, Yasunobu Nakamura, Jaw-Shen Tsai, and William D. Oliver, Noise spectroscopy through dynamical decoupling with a superconducting flux qubit, Nat. Phys. **7,** 565 (2011).

[19] Javier Cerrillo and Jianshu Cao, Non-Markovian Dynamical Maps: Numerical Processing of Open Quantum Trajectories, Phys. Rev. Lett. **112,** 110401 (2014).

[20] Yu-Qin Chen, Kai-Li Ma, Yi-Cong Zheng, Jonathan Allcock, Shengyu Zhang, and Chang-Yu Hsieh, Non-Markovian Noise Characterization with the Transfer Tensor Method, Phys. Rev. Appl. **13,** 034045 (2020).

[21] Jonas Helsen, Francesco Battistel, and Barbara M. Terhal, Spectral quantum tomography, NPJ Quantum Inf. **5,** 1 (2019).

[22] R. C. Bialczak, M. Ansmann, M. Hofheinz, E. Lucero, M. Neeley, A. D. O'Connell, D. Sank, H. Wang, J. Wenner, M. Steffen, A. N. Cleland, and J. M. Martinis, Quantum process tomography of a universal entangling gate implemented with Josephson phase qubits, Nat. Phys. **6,** 409 (2010).

[23] T. Yamamoto, M. Neeley, E. Lucero, R. C. Bialczak, J. Kelly, M. Lenander, Matteo Mariantoni, A. D. O'Connell, D. Sank, H. Wang, M. Weides, J. Wenner, Y. Yin, A. N. Cleland, and John M. Martinis, Quantum process tomography of two-qubit controlled-Z and controlled-NOT gates using superconducting phase qubits, Phys. Rev. B **82,** 184515 (2010).

[24] Andrey V. Rodionov, Andrzej Veitia, R. Barends, J. Kelly, Daniel Sank, J. Wenner, John M. Martinis, Robert L. Kosut, and Alexander N. Korotkov, Compressed sensing quantum process tomography for superconducting quantum gates, Phys. Rev. B **90,** 144504 (2014).

[25] Joel Yuen-Zhou, Jacob J. Krich, Masoud Mohseni, and Alan Aspuru-Guzik, Quantum state and process tomography of energy transfer systems via ultrafast spectroscopy, Proc. Natl. Acad. Sci. **108,** 17615 (2011).

[26] M. Howard, J. Twamley, C. Wittmann, T. Gaebel, F. Jelezko, and J. Wrachtrup, Quantum process tomography and linblad estimation of a solid-state qubit, New J. Phys. **8,** 33 (2006).

[27] A. G. Kofman and A. N. Korotkov, Two-qubit decoherence mechanisms revealed via quantum process tomography, Phys. Rev. A **80,** 042103 (2009).

[28] R. Rosenbach, J. Cerrillo, S. F. Huelga, J. Cao, and M. B. Plenio, Efficient simulation of non-Markovian system-environment interaction, New J. Phys. **18,** 023035 (2016).

[29] Heinz-Peter Breuer and Francesco Petruccione, *The Theory of Open Quantum Systems* (Oxford University Press, New York, 2007).

[30] M. Buser, J. Cerrillo, G. Schaller, and J. Cao, Initial system-environment correlations via the transfer-tensor method, Phys. Rev. A **96,** 062122 (2017).

[31] Christopher King and Mary Beth Ruskai, Minimal entropy of states emerging from noisy quantum channels, IEEE Trans. Inf. Theory **47,** 192 (2001).

[32] L. J. Landau and R. F. Streater, On Birkhoff's theorem for doubly stochastic completely positive maps of matrix algebras, Linear Algebra Appl. **193,** 107 (1993).

[33] A Fujiwara and P Algoet, Affine parameterization of completely positive maps on a matrix algebra, Phys. Rev. A **59,** 3290 (1999).

[34] Ángel Rivas, Susana F. Huelga, and Martin B. Plenio, Entanglement and Non-Markovianity of Quantum Evolutions, Phys. Rev. Lett. **105,** 050403 (2010).

[35] Yijing Yan and Xu RuiXue, Quantum mechanics of dissipative systems, Annu. Rev. Phys. Chem. **56,** 187 (2005).

[36] Michael R. Geller and Zhongyuan Zhou, Efficient error models for fault-tolerant architectures and the Pauli twirling approximation, Phys. Rev. A **88,** 012314 (2013).

[37] R. Harper, S. T. Flammia, and J. J. Wallman, Efficient learning of quantum noise, Nat. Phys. **16,** 1184 (2020).

[38] M. J. Biercuk, H. Uys, A. P. VanDevender, N. Shiga, W. M. Itano, and J. J. Bollinger, Optimized dynamical decoupling in a model quantum memory, Nature **458,** 996 (2009).

[39] Ł. Cywiński, R. M. Lutchyn, C. P. Nave, and S. D. Sarma, How to enhance dephasing time in superconducting qubits, Phys. Rev. B **77,** 174509 (2008).

[40] H. Ball, M. Biercuk, A. Carvalho, J. Chen, M. R. Hush, L. A. De Castro, L. Li, P. J. Liebermann, H. Slatyer, and C. Edmunds *et al.*, Software tools for quantum control: Improving quantum computer performance through noise and error suppression, Quantum Sci. Technol., 2021.

[41] D. Kielpinski, V. Meyer, M. Rowe, C. A. Sackett, W. M. Itano, C. Monroe, and D. J. Wineland, A decoherence-free quantum memory using trapped ions, Science **291,** 1013 (2001).

[42] D. Felinto, C. Chou, H. De Riedmatten, S. Polyakov, and H. Kimble, Control of decoherence in the generation of photon pairs from atomic ensembles, Phys. Rev. A **72,** 053809 (2005).

[43] C. Roos, G. Lancaster, M. Riebe, H. Häffner, W. Hänsel, S. Gulde, C. Becher, J. Eschner, F. Schmidt-Kaler, and R. Blatt, Bell States of Atoms with Ultralong Lifetimes and Their Tomographic State Analysis, Phys. Rev. Lett. **92,** 220402 (2004).

[44] Y. Nakamura, Y. A. Pashkin, and J. Tsai, Coherent control of macroscopic quantum states in a single-cooper-pair box, Nature **398,** 786 (1999).

[45] M. Urbanek, B. Nachman, V. R. Pascuzzi, A. He, C. W. Bauer, and W. A. de Jong, Mitigating Depolarizing Noise on Quantum Computers with Noise-Estimation Circuits, Phys. Rev. Lett. **127,** 270502 (2021).

[46] J. Vovrosh, K. E. Khosla, S. Greenaway, C. Self, M. Kim, and J. Knolle, Simple mitigation of global depolarizing errors in quantum simulations, Phys. Rev. E **104,** 035309 (2021).

[47] B. Pokharel, N. Anand, B. Fortman, and D. A. Lidar, Demonstration of Fidelity Improvement using Dynamical Decoupling with Superconducting Qubits, Phys. Rev. Lett. **121,** 220502 (2018).